RSC Advances

PAPER

View Article Online
View Journal | View Issue

Cite this: *RSC Adv.*, 2019, **9**, 41218

Rhodopseudomonas palustris-based conversion of organic acids to hydrogen using plasmonic nanoparticles and near-infrared light†

John Craven,[a] Mansoor A. Sultan,[b] Rupam Sarma,[a] Sarah Wilson,[a] Noah Meeks,[d] Doo Young Kim,[c] J. Todd Hastings[b] and Dibakar Bhattacharyya *[a]

The simultaneous elimination of organic waste and the production of clean fuels will have an immense impact on both the society and the industrial manufacturing sector. The enhanced understanding of the interface between nanoparticles and photo-responsive bacteria will further advance the knowledge of their interactions with biological systems. Although literature shows the production of gases by photobacteria, herein, we demonstrated the integration of photonics, biology, and nanostructured plasmonic materials for hydrogen production with a lower greenhouse CO_2 gas content at quantified light energy intensity and wavelength. Phototrophic purple non-sulfur bacteria were able to generate hydrogen as a byproduct of nitrogen fixation using the energy absorbed from visible and near-IR (NIR) light. This type of biological hydrogen production has suffered from low efficiency of converting light energy into hydrogen in part due to light sources that do not exploit the organisms' capacity for NIR absorption. We used NIR light sources and optically resonant gold–silica core–shell nanoparticles to increase the light utilization of the bacteria to convert waste organic acids such as acetic and maleic acids to hydrogen. The batch growth studies for the small cultures (40 mL) of *Rhodopseudomonas palustris* demonstrated >2.5-fold increase in hydrogen production when grown under an NIR source (167 ± 18 μmol H_2) compared to that for a broad-band light source (60 ± 6 μmol H_2) at equal light intensity (130 W m^{-2}). The addition of the mPEG-coated optically resonant gold–silica core–shell nanoparticles in the solution further improved the hydrogen production from 167 ± 18 to 398 ± 108 μmol H_2 at 130 W m^{-2}. The average hydrogen production rate with the nanoparticles was 127 ± 35 μmol L^{-1} h^{-1} at 130 W m^{-2}.

Received 24th October 2019
Accepted 28th November 2019

DOI: 10.1039/c9ra08747h

rsc.li/rsc-advances

Introduction

The significant decarbonization of the global energy economy may require the conversion of waste to valuable fuels and other natural resources to meet energy demands at distant times and places. Additionally, the challenge of distributing clean energy may enable the development of on-site energy production from clean sources for remote energy needs. Hydrogen is appealing as it is the most energy dense carrier (122 kJ g^{-1}), and it has no carbon emissions at the point of use.[1,2] As a result, intensive research has been conducted on non-biological, semiconductor-based photocatalytic hydrogen production.[3–5] To mitigate the environmental as well as the economic concerns, ideally, hydrogen must be produced under mild operating conditions from sustainable and renewable resources such as organic waste from food and agricultural sources. It is well reported in the literature that volatile fatty acids (VFAs) such as acetic acid can be easily produced by the anaerobic digestion of municipal sludge, food waste, *etc.*[6–9] These can be converted to molecular hydrogen and carbon dioxide by photofermentation, a biological process in which photosynthetic bacteria metabolize organic acids. Photofermentation is typical for photosynthetic bacteria such as purple non-sulfur bacteria (PNSB), which produce nitrogenase, the key enzyme for hydrogen generation, under nitrogen-limited conditions.[10] The coupling of dark and photofermentative pathways, either by sequencing dark and light cultures or coculturing different types of organisms, is frequently proposed as a way to expand the range of feedstocks available for hydrogen production.[11,12]

Rhodopseudomonas palustris (*R. palustris*) is a purple non-sulfur bacterium widely studied for hydrogen production due to its metabolic diversity and ability to undergo phototrophic or chemotrophic growth using organic or inorganic carbon

[a]*Department of Chemical and Materials Engineering, University of Kentucky, 177 FPAT Bldg, Lexington, KY 40506, USA. E-mail: db@uky.edu; Tel: +1 859 312 7790*

[b]*Department of Electrical and Computer Engineering, University of Kentucky, Lexington, KY 40506, USA*

[c]*Department of Chemistry, University of Kentucky, Lexington, KY 40506, USA*

[d]*Southern Company Services, Inc., Birmingham, AL 35203, USA*

† Electronic supplementary information (ESI) available. See DOI: 10.1039/c9ra08747h

sources.[13] Compared to green algae, which grow photoautotrophically and may produce hydrogen as a result of water splitting,[11] PNSB studied for hydrogen production are typically grown in a photoheterotrophic mode, utilizing organic carbon as a source of electrons. PNSB are capable of sustaining growth using VFAs,[13] carbohydrates[14] and lignin monomers[15] as carbon sources.

The production of hydrogen in PNSB is normally a side reaction of nitrogen fixation. Under nitrogen-limited conditions, the nitrogenase enzyme reduces N_2 to NH_3 according to reaction (1). In the absence of N_2, nitrogenase acts only to produce H_2 (reaction (2) and Fig. 1b).[16] The typical rates of hydrogen production for *R. palustris* range from 10 to 40 mL H_2 per L culture per hour and vary due to the differences in the growth media, illumination and reactor geometry. This process is energy-intensive and highly regulated; aerobic conditions or excess NH_3 can result in the downregulation of nitrogenase activity and reduced hydrogen production.

$$N_2 + 8H^+ + 8e^- + 16ATP \rightarrow 2NH_3 + H_2 + 16ADP \quad (1)$$

$$8H^+ + 8e^- + 16ATP \rightarrow 4H_2 + 16ADP \quad (2)$$

The energy driving this process is supplied by the light-harvesting complexes on the bacterial membrane. Light is absorbed by bacteriochlorophylls present in PNSB and they absorb light in both visible and near-infrared (NIR) regions, with peak absorbance for *R. palustris* around 590, 800, and 850 nm (Fig. 2b). Previously, various illumination strategies have been used to increase hydrogen production. Flat plate reactors can be used to maintain high illumination intensity throughout the culture;[17] also, single-wavelength LEDs have been selected to match the bacteriochlorophyll absorption. The LEDs chosen to match the visible absorption around 590 nm have shown significant improvements in the biomass and hydrogen production compared to the LEDs at 470 or 630 nm, which do not match the bacteriochlorophyll absorption.[18]

There has also been interest in targeting the absorption of longer wavelength light by bacteriochlorophyll absorption peaks above 800 nm. Hydrogen production by the cultures of *Rhodobacter sphaeroides*, another PNSB, decreased by 43% when light above 760 nm was filtered from a tungsten lamp compared to only 7% decrease when light below 630 nm was filtered.[19] Another group compared commonly used tungsten lamps to an NIR LED array without matching intensity and found that the NIR illumination led to increased bacterial growth and initial hydrogen production but resulted in similar total hydrogen generation.[20] Turon *et al.* compared hydrogen production rates from a different species, *Rhodobacter capsulatus*, using different light sources and found that visible + NIR performed better than

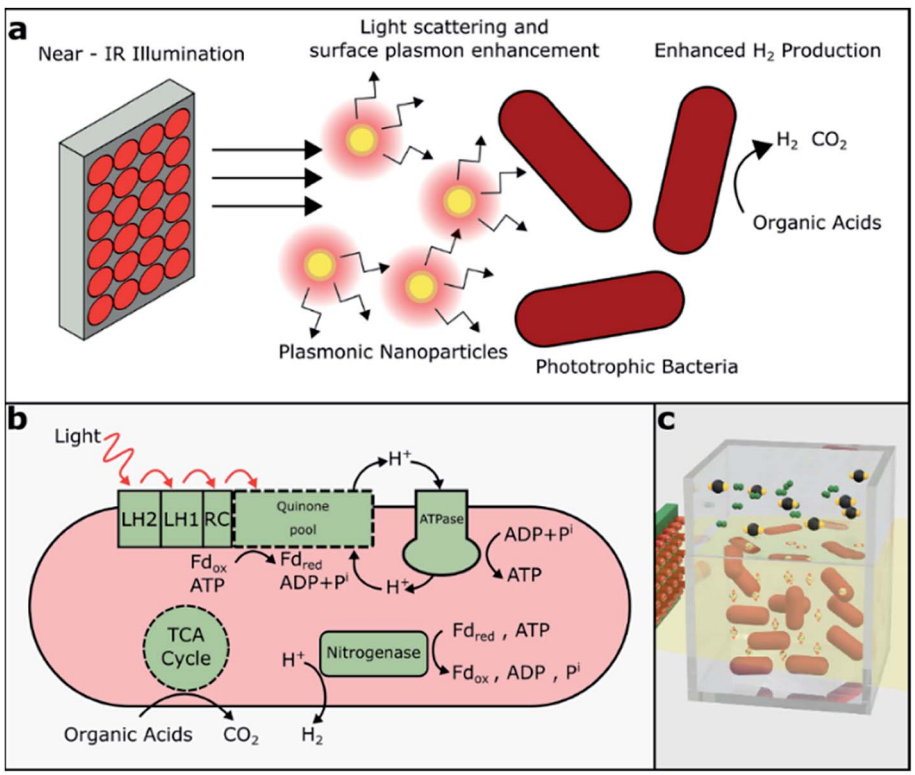

Fig. 1 Experimental scheme and reaction pathway. (a) NIR illumination was used as a light source for growing PNSB (*R. palustris*). The silica–gold core–shell plasmonic nanoparticles further enhanced the biohydrogen production in solution through light scattering and surface plasmon effects. (b) Overview of the metabolic process of *R. palustris* under photoheterotrophic nitrogen fixing conditions. Abbreviations: LH1, LH2 = light harvesting complexes; RC = reaction center; Fd = ferredoxin (oxidized, reduced); adapted from (13). (c) 3D drawing of bacteria and nanoparticles in suspension with evolved CO_2 and H_2 in the headspace.

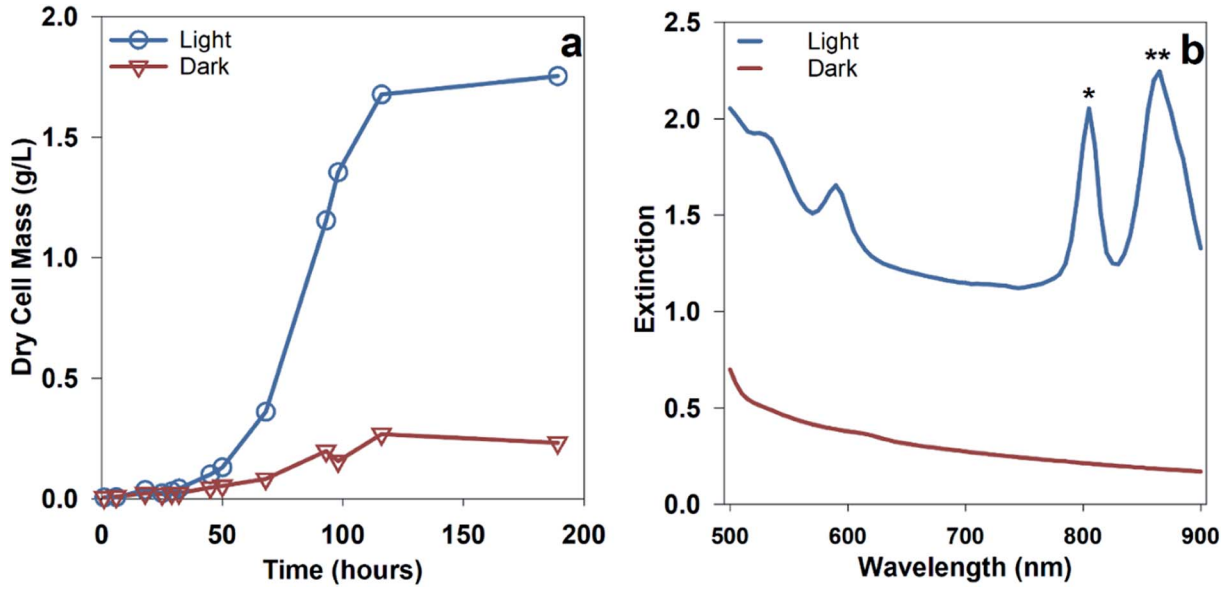

Fig. 2 Cell growth and extinction spectra under illuminated and dark conditions. (a) Anaerobic growth of *R. palustris* in 20 mL minimal media at 30 °C using 70 mM acetate as a carbon source and white LED (20 W m^{-2}) for samples grown in light. Samples grown in dark were covered in an aluminum foil. (b) Sample extinction spectrum for *R. palustris* grown anaerobically under dark and light conditions after 90 hours. Only the samples grown in light conditions exhibited bacteriochlorophyll absorption peaks near 800 and 850 nm. Bacteriochlorophyll (*) = B800 (**) = B850, B875.

NIR illumination alone.[21] Again, the intensity of the light sources did not match, which made the direct comparison of the light-to-hydrogen conversion efficiency difficult. Finally, we are unaware of prior studies that have compared hydrogen generation from the species considered here, namely, *R. palustris* under visible *versus* NIR illumination.

Another method of increasing light utilization that has not yet been explored is the exploitation of the photonic properties of plasmonic nanoparticles to increase light absorption in phototrophic bacteria (Fig. 1a). Plasmonic nanoparticles, particularly gold and silver, exhibiting localized surface plasmon resonance (LSPR) have been widely studied for their use in biosensing, cellular imaging, cancer therapy,[22] and solar-cell enhancement.[23,24] LSPR represents the collective oscillations of free electrons driven by photons at resonant wavelengths larger than the size of the particle. These localized plasmon oscillations enhance the electric near-field around the particle, and they strongly depend on the particle's material and the surrounding media.[25] Plasmonic nanoparticles also often exhibit absorption and scattering cross-sections significantly greater than their cross-sectional areas. Absorption tends to prevail in smaller nanoparticles, whereas scattering dominates in larger nanoparticles.[26]

We hypothesized that narrow-band NIR illumination with appropriate intensity will allow a higher bacterial growth rate and higher hydrogen production from *R. palustris* than broadband illumination of the same intensity. In contrast to previous studies, we quantified the relative hydrogen generation from *R. palustris* rather than *R. sphaeroides* or *R. capsulatus* under broadband (visible and NIR) *versus* narrow-band NIR illumination. Also, unlike prior works, we matched the intensities of the broadband and NIR light sources to remove any intensity-dependent effects and more directly compare the light-to-hydrogen conversion efficiency. In addition, we expect that the novel approach of adding nanoparticles with LSPRs matched to the NIR source and the bacteriochlorophyll absorption peaks will further enhance hydrogen production through light scattering and/or near-field enhancement. Here, we showed that NIR illumination did, in fact, enhance hydrogen production over broadband illumination when the intensities were matched and that core–shell nanoparticles with LSPRs tuned to the NIR bacteriochlorophyll absorption peaks enhanced hydrogen production even further.

Results & discussion

Impact of the light source on bacteria culturing and H_2 production

Hydrogen production from PNSB predominantly occurs during illuminated growth under anaerobic, nitrogen-fixing conditions. As seen in Fig. 2a, the dark anaerobic growth in the defined media using acetate as a carbon source only reached a maximum culture concentration of 0.27 g dry cell mass (DCM) per L compared to that for the cultures illuminated with 20 W m^{-2} white LED. Because this medium was not rich in the nutrients necessary to sustain chemoheterotrophic growth, the bacteria required energy from light to grow. Growth using different media types including complex media having soy broth or yeast extract is shown in ESI Fig. 1.† The illuminated cultures also developed red pigmentation associated with photocenters for light absorption. The bacteriochlorophyll absorption (B800, B850) shown in Fig. 2b is a result of the light-harvesting complexes on the bacterial membrane.[13]

We were interested in determining if the illumination of an NIR source alone results in increased hydrogen production for *R. palustris*. We expected that shifting the illumination intensity to the NIR photoactive region would result in increased metabolic activity. To determine the effect of shifting the wavelength of illumination, parallel batch cultures were grown using two different light sources: a broad tungsten source and an NIR LED array centered around 850 nm, as shown in Fig. 3a, which showed hydrogen production of 60 ± 6 μmol with broadband light and 167 ± 18 μmol with NIR LED. Over the first 90 hours, including the lag and exponential growth phases, the average hydrogen production rate with NIR illumination was 62 ± 7 μmol L^{-1} h^{-1} (89 ± 18 μmol (g bacteria)$^{-1}$ h^{-1}). The spectral overlap between the broadband and NIR LED light sources with the bacteriochlorophylls is shown in Fig. 3b and c. The variance in the intensities of these light sources can be found in ESI Fig. 3.† The cultures illuminated with NIR LEDs produced almost 3 times more hydrogen than those illuminated with a broad light source. This was expected at light intensities below the saturation limit, where shifting illumination to preferentially absorbed spectral regions would increase the available energy and reductive potential within the bacteria and increase the metabolic activity. The increased metabolic activity also resulted in an increase in the cell density, with the cultures illuminated with NIR LEDs reaching a final cell concentration 1.5 times higher than that for the cultures illuminated with a broadband light source.

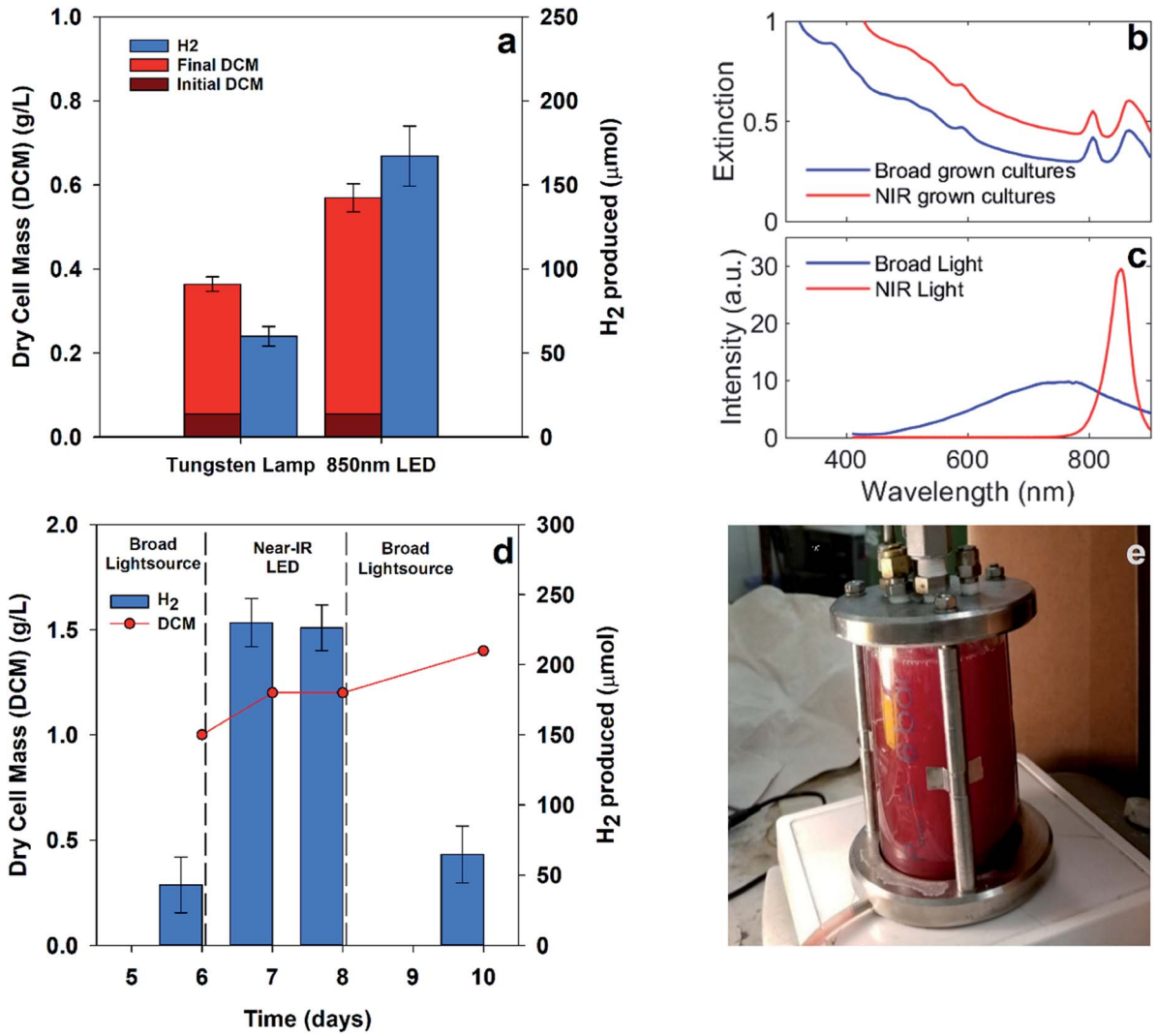

Fig. 3 Enhancement of hydrogen production under near IR illumination. (a) Batch growth in 40 mL PTFE/silicone septa vials illuminated with an NIR LED array (850 nm) or a tungsten lamp (peak 660 nm, broadband) for 90 hours at an intensity of 130 W m^2; $n = 4$ vials per illumination source. All vials were incubated at 30 °C and shaken at 100 rpm in an orbital shaker. The cultures illuminated with the NIR LED array showed increased cell growth and hydrogen generation compared to the cultures illuminated with a broad wavelength lamp. (b) Extinction spectra for cultures grown (a) under two light sources. (c) Light intensity spectra for the two light sources used in (a). (d) *R. palustris* cultured in a 300 mL reactor under a broad light source (tungsten lamp), then switched to illumination using an 850 nm LED array for 2 days, and switched back to the broad light source. The illumination intensity for both sources was adjusted to the range of 82–91 W m^{-2}, and the culture was maintained at 22 °C. Hydrogen production represents the headspace collection over 24 h; $n = 3$ headspace measurements (e) membrane reactor (300 mL) with the *R. palustris* culture. Error bars represent standard deviations.

To further establish the efficacy of targeted illumination for increasing hydrogen production in PNSB, we compared the effect of switching light sources on a single pre-grown 0.3 liter culture, as shown in Fig. 3e. Fig. 3d shows the results of pre-growing a culture of *R. palustris* under broad illumination, switching to NIR LEDs of matched intensity, and switching back to broad illumination. Each measurement of hydrogen represents 3 samples from the headspace of one reactor after gas collection for 24 hours. The culture density increased by 40% over the entire measurement period, but the hydrogen production was around 3.5–5× higher under NIR LED illumination. These increased values are comparable to those in Fig. 3a despite the increased culture size. This showed that the increase in the hydrogen production efficiency under NIR LEDs was not solely due to an increase in the culture density.

Comparisons between illumination sources using other PNSB species had varying results. Kawagoshi *et al.* using a 200 mL culture of *Rhodobacter sphaeroides* found that illumination with NIR LED resulted in a higher initial growth rate and hydrogen production rate compared to that for a tungsten bulb (about 2× more hydrogen production from the NIR LED after the first 100 hours).[20] This resulted in about 2× more hydrogen production for the NIR illuminated culture after the first 100 hours but only 1.3× increase in the cumulative hydrogen production over the entire course of the experiment. The intensity of the tungsten source was estimated to be about four times that of the NIR source for these studies. In contrast, our studies with matched intensities still showed a significant enhancement in the hydrogen production after 8 days.

Our results also contrasted with those presented by Turon *et al.*, who found that NIR illumination only resulted in around half of the total hydrogen production of a 1 L culture of *Rhodobacter capsulatus* compared to that for incandescent (300–1100 nm) illumination. They attributed the drop in performance to self-shading effects; the NIR light was preferentially absorbed at the illuminated surface of the container, leaving deeper parts of the culture under-illuminated and decreasing the total hydrogen production.[21] In contrast, our experiments used a smaller culture size, *i.e.*, 30 mL compared to 1 L and lower intensity illumination, *i.e.*, 130 W m^{-2} compared to 1150 W m^{-2}. The smaller culture size could diminish the effects of self-shading and lead to reversal in the efficacy of NIR illumination, as shown in Fig. 3a. These results underscore that effective light distribution within a culture, particularly in dense cultures, is critical for maintaining hydrogen production.

Reduced CO_2 production

Hydrogen production from the photofermentation of organic substrates results in the concurrent production of CO_2. The complete oxidation of the electron donor results in varying theoretical ratios of H_2 : CO_2, as shown in eqn (1) and (2) for acetic and malic acid, respectively. PNSB can also fix CO_2 through the Calvin cycle, which may reduce the net amount of CO_2 produced.[13] Mckinlay *et al.* studied the metabolism of *R. palustris* in different phases of growth and found that growing cultures of *R. palustris* tended to use the glyoxylate cycle over the TCA cycle, thus conserving carbon and reducing CO_2 generation at the cost of generating fewer reduced electron carriers.[29] Carbon fixation through the Calvin cycle is one major electron sink for autotrophic organisms, and it competes with nitrogen fixation for electron carriers within the cell.[30] In a separate study by Mckinlay *et al.* using a wild type and mutant *R. palustris* strain in which nitrogenase was not downregulated by ammonia, it was shown that the Calvin cycle gene expression and flux decreased significantly in the strain with high nitrogenase activity.[31]

To test the extent of CO_2 production, we compared H_2 and CO_2 production using two organic acid substrates. Fig. 4a shows the gas collected over 24 hours from a culture of *R. palustris* grown using acetate as a sole carbon source. Much less CO_2 was measured than the expected value from the stoichiometry of acetate with a ratio of H_2 : CO_2 of 33 : 1 compared to the theoretical ratio of 2 : 1. Using malate as a sole carbon source, the culture showed decreased CO_2 production throughout the growth phase, resulting in a final cumulative ratio of 36 : 1, as shown in Fig. 4b. The low amount of CO_2 production in these results could be due to the predominance of the glyoxylate cycle over the TCA cycle, the continued carbon fixation through the Calvin cycle in spite of nitrogenase activity, or a combination of these two pathways. Turon *et al.* also found high hydrogen concentrations in the evolved gas from the *Rhodobacter capsulatus* cultures based on the above theoretical expectations with the evolved gas consisting of 97–99% H_2.[21]

$$C_2H_4O_2 + 2H_2O \rightarrow 2CO_2 + 4H_2 \quad (3)$$

$$C_4H_6O_5 + 3H_2O \rightarrow 4CO_2 + 6H_2 \quad (4)$$

Nanoparticle enhancement of the light intensity for hydrogen generation

Localized surface plasmons are the collective oscillations of free electrons that lead to charge oscillations on the surface of nanostructures. These oscillations can be driven by optical photons, particularly those with wavelengths near the localized surface plasmon resonance (LSPR). The resonance wavelength can be tuned by changing the geometry and optical properties of the nanoparticles as well as the properties of the surrounding media.[25] For resonance, localized surface plasmon oscillations enhance the electromagnetic near-field around the particles and increase both the absorption and scattering cross-sections. In many cases, the absorption and scattering efficiencies, the ratio of the optical to physical cross-sections, can exceed one. Nanoparticles exhibiting LSPR have widely been studied for applications including solar cells, drug delivery, pollutant degradation, and affinity sensing.[32–35] Both near-field enhancement and light trapping through efficient scattering from these nanoparticles can improve the efficiency of light-harvesting systems.

Our approach utilized nanoparticles with localized surface-plasmon resonance wavelengths around the NIR absorption maxima of bacteriochlorophylls. Specifically, we used

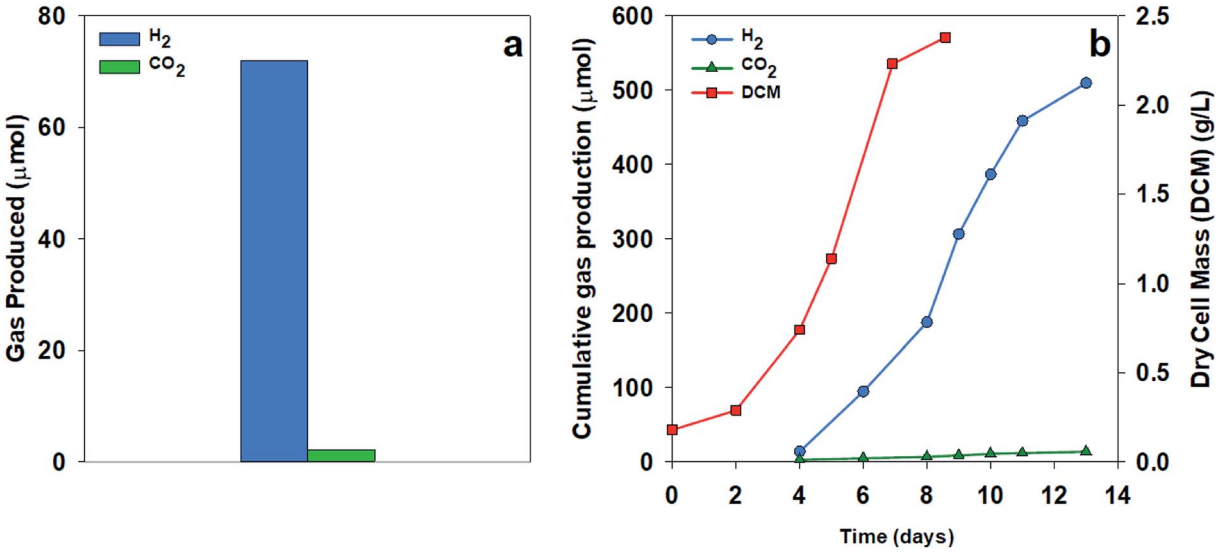

Fig. 4 CO_2, H_2, production, and cell mass of *R. palustris* using two substrates. Cultures of *R. palustris* (300 mL) grown anaerobically at 22 °C using 850 nm LED array illumination adjusted to 82–91 W m^{-2} (a) Acetate (70 mM) as a carbon source with the gas concentration in the headspace collected over 24 h after 48 h growth. (b) Malate (70 mM) as a carbon source; for each measurement, the headspace was flushed with N_2.

nanoparticles with a silica core and a gold shell, an example of which is shown in the cross-section in Fig. 5a.[36,37] These core–shell particles enhanced the optical near-field, potentially leading to more efficient coupling to the light-harvesting complexes in the bacteriochlorophylls. In addition, they offered relatively high scattering cross-sections with relatively low absorption cross-sections, as discussed in the ESI.† This property enhanced light trapping in the reactor due to efficient scattering while reducing light lost to particle absorption.

The preliminary particle selection was based on Mie theory calculations of the optimum extinction cross-section area at the NIR region.[38] The optimum particles were silica–gold core–shell structures (~160 nm silica core, ~18 nm gold shell). These particles had a broad extinction peak around 850 nm that was primarily due to scattering (ESI Fig. 7†). Other shapes of the particles could also serve the purpose such as nano-rods,[39] rings,[40] and cages[41] or various passivated copper structures.[42] The experiments conducted here used particles with a nominal silica core diameter of 120 nm ± 9 nm, a gold shell diameter of 16 nm, a 5 kDa mPEG coating, and a total diameter of 151 nm ± 8 nm (NanoXact from nanoComposix Inc.). The cross-sectional electron micrograph in Fig. 5a reveals the core–shell structure.

Fig. 5b shows the calculated and measured extinction cross-section of these particles, which was dominated by scattering as noted above. Calculations were conducted using the finite difference time domain method and are detailed in the ESI.† As expected, the extinction maximum associated with LSPR is centered at 800 nm and spans both of the NIR bacteriochlorophyll absorption maxima. The measured and calculated spectral shapes were similar and both the antisymmetric (~600 nm) and symmetric (~800 nm) resonances were apparent. The experimentally measured resonances broadened and damped compared to the calculated resonances likely because of the geometric heterogeneity and aggregation of some particles in solution. The calculated field enhancement around the particle is shown in the inset in Fig. 5b. The maximum field enhancement is 7× and the near-field decays over a distance of approximately 30 nm from the particle's surface.

These particles exhibited the desired near-field enhancement and efficient scattering near the bacteriochlorophyll extinction maxima. Thus, two experiments were conducted to quantify the enhancement of hydrogen production by *R. palustris* in the presence of the gold nanoparticles. In both experiments, the nanoparticles were dosed into the samples at a concentration of 4.6 μg mL^{-1} (equivalent to 2.6×10^8 particles per mL).

To test the efficacy of these nanoparticles for enhancing the light absorption of *R. palustris*, cultures were grown under NIR LEDs with gold nanoparticles in solutions, as shown in Fig. 5c. The broad spectral overlap of the nanoparticle extinction and the bacteriochlorophyll absorption can be seen in Fig. 5d and e. The addition of the nanoparticles resulted in a similar cell growth but more than 2× increase in hydrogen production over 90 hours from 167 ± 18 to 398 ± 108 μmol H_2 in the 40 mL reaction vial. This was in addition to the enhancements from the illumination with NIR LEDs. The average hydrogen production rate with the nanoparticles (total liquid volume of 34 mL) was 127 ± 35 μmol L^{-1} h^{-1} at 130 W m^{-2}. Previous results using acetate as well as mixed organic substrates with various light sources yielded hydrogen production rates ranging from 84 μmol L^{-1} h^{-1} to 1800 μmol L^{-1} h^{-1}.[16,27,28] The higher reported production rates arose from advanced reactor and illumination designs,[16] which made the comparison difficult with the simple vials and direct illumination employed here. Moreover, we did not attempt to optimize the media, substrate concentration, or mixing in these experiments. Thus, combining NIR LED illumination, resonant nanoparticles, and advanced reactors should ultimately increase the overall production rate.

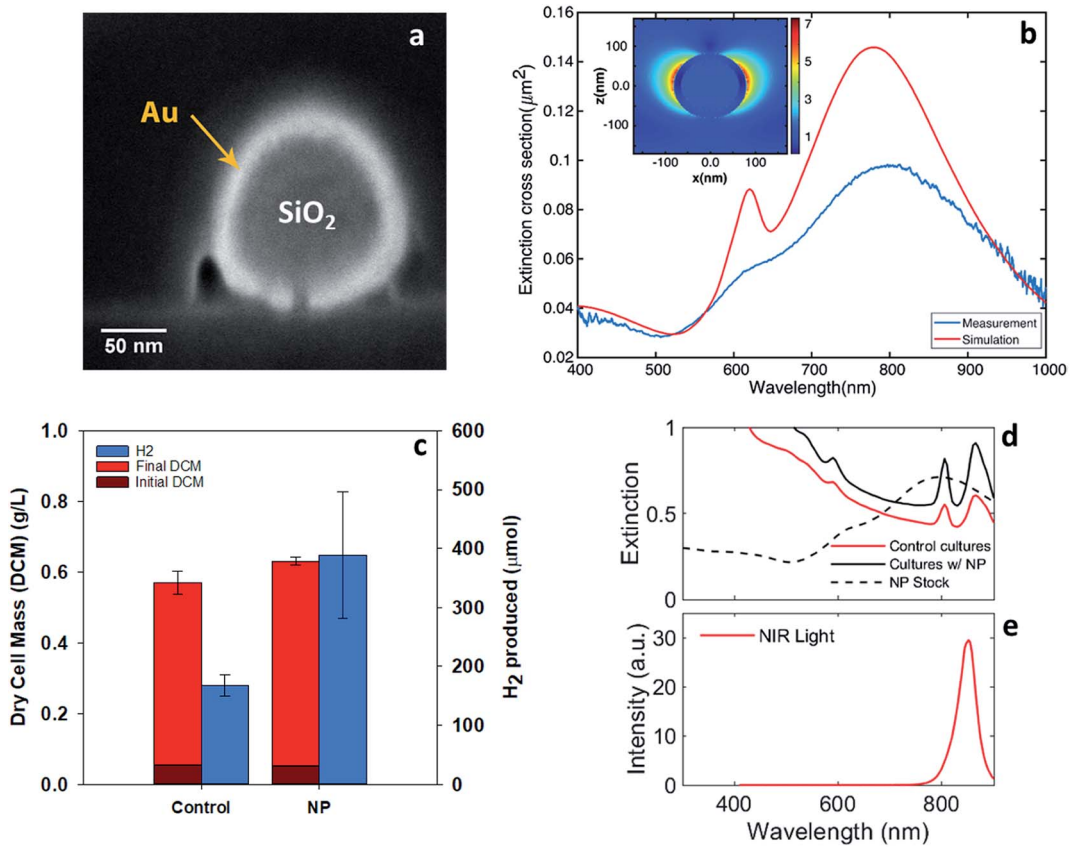

Fig. 5 Role of gold-shell nanoparticles on the enhancement of hydrogen production. (a) The silica-core, gold-shell nanoparticle cross-section. The scale bar is 50 nm and the shell thickness is approximately 18 nm. The particles were coated with mPEG (methoxy polyethylene glycol) and had a 188 nm hydrodynamic diameter. (b) Extinction cross-section simulation and measurement. The inset shows the modeled near-field enhancement. (c) Dry cell mass and hydrogen production from batch growth in 40 mL PTFE/silicone septa vials illuminated with an NIR LED array (850 nm) for 90 hours at an intensity of 130 W m^{-2} ($n = 4$ vials per illumination source). For the NP vials, the culture media contained 2.64×10^8 particles per mL. All vials were incubated at 30 °C and shaken at 100 rpm in an orbital shaker. The dry cell mass was estimated by correlating the optical density at 660 nm. Error bars represent standard deviations. (d) Extinction spectra for the control and nanoparticle-dosed cultures from (c) as well as the nanoparticle stock in DI H_2O (2.9×10^9 particles per mL). (e) Light spectra for the NIR LED light used for both sets of cultures in (c).

The simulations of the nanoparticles alone, shown in ESI Fig. 10b,† predict some absorption of light, which can theoretically impact the bulk temperature of the culture and hydrogen production. The nanoparticles being added to media alone and illuminated similar to the experiments presented in Fig. 5 only increased the bulk temperature by 0.8 °C compared to that for the media without nanoparticles, as detailed in ESI Table 3.† Furthermore, as shown in ESI Fig. 10,† two sets of bacteria were illuminated with the NIR LED arrays at 25 and 40 °C and the elevated temperature led to a significant reduction in the hydrogen production. This agreed with the results by Wang *et al.*[28] who conducted visible light illumination studies with *R. palustris*, where the optimum temperature for hydrogen production was 30 °C and it dropped significantly at 40 °C. Because the experiments conducted, as shown in Fig. 5c, were held constant at 30 °C using an incubator, we do not believe that the increase in the hydrogen production from the addition of the nanoparticles was due to the heating effects from the presence of the nanoparticles.

Although gold nanoparticles have been studied as a means to kill cancer cells through photothermal conversion,[43] cell growth was not impeded here from the addition of nanoparticles because the intensity of light used was small compared to the light intensity typically used for cancer treatment. Additionally, the 5 kDa mPEG coating served as a barrier between the nanoparticles and bacteria.

Conclusion

Here, we demonstrated the efficacy of NIR illumination for PNSB (photorophic non-sulfur bacteria) growth and hydrogen production. Switching to NIR illumination compared to the widely used tungsten light sources resulted in 3-fold increase in the hydrogen production (60 ± 6 to 167 ± 18 μmol H_2 at 130 W m^{-2}). Furthermore, the addition of the mPEG-coated plasmonic nanoparticles in the solution resulted in additional 2-fold increase in the hydrogen production (167 ± 18 to 398 ± 108 μmol H_2) with minimal inhibition of the bacterial growth. Another key finding of our work established that part of the generated CO_2 was simultaneously utilized by the bacteria, resulting in a higher purity hydrogen gas.

The increased understanding of plasmonic materials can also be used to better understand the light absorption and

energy transfer processes of phototrophic organisms. Various studies have examined the strong coupling between light-harvesting complexes from plants and bacteria to extended gold arrays.[44–46] The results by Tsargorodska *et al.* examined the strong coupling between the extracted wild type light-harvesting complexes of *R. sphaeroides*, another PNSB, and plasmonic gold nanostructure arrays.[46] Coles *et al.* even demonstrated strong coupling between a phototrophic green sulfur bacterium and a photonic microcavity.[47] Although strong coupling was not expected in our work, where the nanoparticles were suspended in the solution and there were no observed changes in the extinction spectra, its impact on the hydrogen production will be an important avenue for future investigations. Outside gold nanoparticles, Wang *et al.* studied the effects of CdS nanoparticles on *R. palustris* and found significant improvements in the cell growth, hydrogen production, and nitrogen fixation.[48] This work differs in the selection of nanoparticles, which exhibit optical scattering in the same wavelength range as that for bacteriochlorophyll absorption.

Other research studies on supplementing biohydrogen production with nanoparticles have also shown improved hydrogen production, but these studies have mostly focused on dark fermentative bacteria.[49,50] For example, Zhang *et al.* used intracellular gold nanoclusters to photosensitize a non-photosynthetic bacterium, *M. thermoacetica*, and enable CO_2 fixation by absorbing light energy and transferring energized electrons into the Wood–Ljungdahl pathway.[51] The immobilization of bacteria and nanoparticles in close proximity could more effectively exploit near-field enhancement and perhaps strong coupling effects.

Experimental: materials and methods

Microorganism and culture conditions

The *R. palustris* strain CGA009 (ATCC BAA-98) was purchased from ATCC (American Type Culture Collection). Solid media cultures were isolated on tryptic soy broth agar plates. Liquid cultures were pre-grown anaerobically in tryptic soy broth purchased from Criterion, which contained (g L^{-1}) casein peptone, 17; soy peptone, 3; NaCl, 5; K_2HPO_4, 2.5; and dextrose, 2.5. The pre-grown liquid cultures were concentrated by centrifugation at 2500 rpm for 5 minutes and washed 3 times with minimal media for use as an inoculant for the hydrogen production experiments. For the hydrogen production experiments, *R. palustris* was grown using modified minimal media[52] that contained (g L^{-1}) Na_2HPO_4, 6.8; KH_2PO_4, 2.9; NaCl, 1.3; $MgSO_4 \cdot 7H_2O$, 0.4; $CaCl_2 \cdot 2H_2O$, 0.075; and thiamine hydrochloride, 0.001. Trace elements were provided by adding 10 mL L^{-1} of a solution containing (g L^{-1}) $FeCl_3 \cdot 6H_2O$, 1.66; $ZnCl_2$, 0.17; $MnCl_2$, 0.06; $CoCl_2 \cdot 6H_2O$, 0.06; $CuCl_2 \cdot 2H_2O$, 0.04; $CaCl_2 \cdot 2H_2O$, 0.73; and $Na_2MoO_4 \cdot 2H_2O$, 0.06. Sodium glutamate (3.5–7 mM) and acetate (70 mM) were utilized. The final concentrations of the transition metals in the defined medium were (mg L^{-1}) Fe, 31.2; Zn, 7.4; Mn, 2.4; Co, 1.4; Cu, 1.4; and Mo, 2.2. To prevent the growth of contaminants in the cell cultures, chloramphenicol was added to the cell culture media in concentrations of 10 mg L^{-1}.

Hydrogen production experiments

Batch hydrogen production experiments were conducted in sets of 40 mL vials with PTFE-lined silicone septa. The vials were shaken on their side at 100 rpm and 30 °C in an orbital shaker. The vials were illuminated from the bottom, and the illumination intensity was tested by measuring with a photometer perpendicular to the vial surface. For the multiple illumination experiments, sets of vials were oriented perpendicular to each other and covered with foils on the non-illuminated sides to minimize cross-illumination.

For larger-scale hydrogen production, a cylindrical glass solvent-resistant stirred cell (EMD-Millipore) with an internal diameter of 76 mm and a working volume of 300 mL was used for these experiments. The culture was stirred with a magnetic stirrer. All experiments were carried out under an anaerobic atmosphere with just above 1 bar pressure. All experiments were carried out under continuous irradiance at 82 ± 10 W m^{-2} with either a broad wavelength incandescent light or LED array.

Light source spectral and power measurements

The spectrum of both light sources (broad wavelength EVA 64623 bulb OSRAM HLX 100 W single-ended tungsten–halogen bulb and NIR-LED source, CMVision CM-IR110 LED array) was measured with an Ocean Optics HR4000CG-UV-NIR spectrophotometer. The measurements were corrected for the efficiency of the optics and spectral response of the CCD sensor. The light power was measured using a light power meter (LabMax-TOP, Coherent Inc.). The broadband light source power was measured at the peak wavelength.

Nanoparticle extinction measurements

Commercially available water suspensions of silica-core gold nanoshells with a resonance wavelength of 800 nm were purchased from NanoCompsix. The core diameter of these particles was 120 ± 9 nm with a shell thickness of 16 nm. These shells were coated with poly(ethylene glycol) methyl ether (mPEG). The extinction spectrum of these particles was measured by an Ocean Optics HR4000CG-UV-NIR spectrophotometer with a reference signal of DI-water, an integration time of 10 milliseconds, and a light path length of 1 cm. Cross-sectioning of the particles and imaging was done using a Thermo Fisher Scientific/FEI dual beam FIB/SEM system (Helios Nanolab 660).

Numerical simulation of optical properties of nanoparticles

Finite different time domain analysis (Lumerical Inc.) was utilized to simulate a suspended particle in water to estimate the resonance wavelength and scattering cross-section. The refractive index for gold was taken from Johnson & Christy[53] and the refractive indices for water and silica were taken from Palik.[54] The best fit model has an error tolerance of 0.1 and a maximum allowed number of coefficients as 6 for gold and 0.01 and 2 for water and silica, respectively (see ESI Fig. 5 and 6† for full details of the material optical properties). The mesh size was set to 1.8 nm to account for surface plasmon effects. The

full mathematical modeling of the core–shell particles can be found in ref. 55.

Nanoparticle addition experiments

Batch experiments to test the enhancement of the growth and hydrogen production from the addition of the commercial gold shell (Au–silica) nanoparticles were carried out in the same manner as the other batch growth experiments. The bacterial cultures were grown in 40 mL vials with 30 mL of minimal media and 1 mL inoculant. In addition, the samples with nanoparticles were dosed with 3 mL of a nanoparticle stock solution, resulting in a final concentration of 4.5 mg L^{-1} nanoparticles. The change in the headspace was taken into account in calculating the total hydrogen generation per sample.

Analytical methods

The total cell concentration was determined by recording the optical density (OD) of the cell culture at 660 nm with a BioTek microplate reader (Synergy H1 Hybrid reader). OD660 was converted to dry weight (g L^{-1}) by gently drying the concentrated samples in replicate at 80 °C until there was no mass change. Dilutions of the concentrated sample were then measured for absorbance.

The hydrogen gas produced by the bacteria cells in the headspace was collected by a luer lock syringe and analyzed by GC (Agilent 6890N) with a Carboxen-1004 micropacked column (0.75 mm × 2 m) equipped with a TCD detector. The column temperature was held at 50 °C for 1 min, then increased to 150 °C at 10 °C min^{-1} and maintained for 5 min. Nitrogen was used as the carrier gas at 1.8 mL min^{-1}. The injector and the detector temperatures were set at 100 °C and 150 °C, respectively. The retention time for hydrogen gas was 1.3 min. A calibration curve was obtained for hydrogen gas in the linear range of 100–1000 ppm. All reported data were the averages of the analysis performed at least in triplicate wherever possible. For the analysis of the CO_2 produced, GC (Varian) equipped with a mass spectrometric detector was used. A two-point calibration with 200 and 400 ppm CO_2 was used for analysis.

Author contributions

JC and RS performed the bacterial experiments and data analysis. MS contributed the nanoparticle modeling work and optical measurements. SW contributed the microbiological experiments and helped establish the growth protocols. NM provided an industrial perspective. DB, DYK, and JTH conceived the work and helped design the experiments. All of the authors contributed to the overall manuscript write-up.

Data availability

The data that support the findings of this study are available from the corresponding author upon reasonable request.

Conflicts of interest

The authors declare no conflict of interest.

Acknowledgements

This material was based upon work supported by the National Science Foundation EAGER grant 1700091 and by NSF EPSCoR grant 1355438. The NSF EAGER grant was awarded in February 2017. Additional financial support was provided by Southern Company. This work was performed in part at the UK Center for Nanoscale Science and Engineering and the UK Electron Microscopy Center, which are members of the National Nanotechnology Coordinated Infrastructure (NNCI). NNCI is supported by the National Science Foundation (ECCS-1542164). This work used equipment supported by the National Science Foundation Grant No. CMMI-1125998.

References

1 A. Yilanci, I. Dincer and H. K. Ozturk, *Prog. Energy Combust. Sci.*, 2009, **35**, 231–244.
2 G. Padovani, S. Vaičiulytė and P. Carlozzi, *Fuel*, 2016, **166**, 203–210.
3 A. Patsoura, D. I. Kondarides and X. E. Verykios, *Catal. Today*, 2007, **124**, 94–102.
4 C. Zhou, C. Lai, C. Zhang, G. Zeng, D. Huang, M. Cheng, L. Hu, W. Xiong, M. Chen and J. Wang, *Appl. Catal., B*, 2018, **238**, 6–18.
5 C. Zhou, P. Xu, C. Lai, C. Zhang, G. Zeng, D. Huang, M. Cheng, L. Hu, W. Xiong and X. Wen, *Chem. Eng. J.*, 2019, **359**, 186–196.
6 A. Alloul, S. Wuyts, S. Lebeer and S. E. Vlaeminck, *Water Res.*, 2019, **152**, 138–147.
7 A. Alloul, R. Ganigué, M. Spiller, F. Meerburg, C. Cagnetta, K. Rabaey and S. E. Vlaeminck, *Environ. Sci. Technol.*, 2018, **52**, 6729–6742.
8 T. Hülsen, E. M. Barry, Y. Lu, D. Puyol and D. J. Batstone, *Water Res.*, 2016, **100**, 537–545.
9 T. Hülsen, K. Hsieh, S. Tait, E. M. Barry, D. Puyol and D. J. Batstone, *Water Res.*, 2018, **144**, 665–676.
10 D. Muzziotti, A. Adessi, C. Faraloni, G. Torzillo and R. De Philippis, *Res. Microbiol.*, 2016, **167**, 350–356.
11 H. Sakurai, H. Masukawa, M. Kitashima and K. Inoue, *J. Photochem. Photobiol., C*, 2013, **17**, 1–25.
12 A. Adessi, E. Corneli and R. De Philippis, in *Modern Topics in the Phototrophic Prokaryotes: Environmental and Applied Aspects*, ed. P. C. Hallenbeck, Springer International Publishing, Cham, 2017, pp. 321–350.
13 F. W. Larimer, P. Chain, L. Hauser, J. Lamerdin, S. Malfatti, L. Do, M. L. Land, D. A. Pelletier, J. T. Beatty, A. S. Lang, F. R. Tabita, J. L. Gibson, T. E. Hanson, C. Bobst, J. L. T. y. Torres, C. Peres, F. H. Harrison, J. Gibson and C. S. Harwood, *Nat. Biotechnol.*, 2004, **22**, 55–61.
14 K.-J. Lo, S.-S. Lin, C.-W. Lu, C.-H. Kuo and C.-T. Liu, *Sci. Rep.*, 2018, **8**, 12769.

15 J. B. McKinlay and C. S. Harwood, *Curr. Opin. Biotechnol.*, 2010, **21**, 244–251.
16 A. Adessi and R. De Philippis, *Int. J. Hydrogen Energy*, 2014, **39**, 3127–3141.
17 K. Skjånes, U. Andersen, T. Heidorn and S. A. Borgvang, *J. Appl. Phycol.*, 2016, **28**, 2205–2223.
18 Q. Liao, Y.-J. Wang, Y.-Z. Wang, X. Zhu, X. Tian and J. Li, *Bioresour. Technol.*, 2010, **101**, 5315–5324.
19 B. Uyar, I. Eroglu, M. Yucel, U. Gunduz and L. Turker, *Int. J. Hydrogen Energy*, 2007, **32**, 4670–4677.
20 Y. Kawagoshi, Y. Oki, I. Nakano, A. Fujimoto and H. Takahashi, *Int. J. Hydrogen Energy*, 2010, **35**, 13365–13369.
21 V. Turon, Z. Anxionnaz-Minvielle and J. C. Willison, *Int. J. Hydrogen Energy*, 2018, **43**, 7784–7794.
22 V. Amendola, R. Pilot, M. Frasconi, O. M. Maragò and M. A. Iatì, *J. Phys.: Condens. Matter*, 2017, **29**, 203002.
23 Z. F. Yu, A. Raman and S. H. Fan, *Proc. Natl. Acad. Sci. U. S. A.*, 2010, **107**, 17491–17496.
24 S. K. Cushing and N. Q. Wu, *J. Phys. Chem. Lett.*, 2016, **7**, 666–675.
25 S. J. Oldenburg, J. B. Jackson, S. L. Westcott and N. Halas, *Appl. Phys. Lett.*, 1999, **75**, 2897–2899.
26 P. K. Jain, K. S. Lee, I. H. El-Sayed and M. A. El-Sayed, *J. Phys. Chem. B*, 2006, **110**, 7238–7248.
27 M. J. Barbosa, J. M. Rocha, J. Tramper and R. H. Wijffels, *J. Biotechnol.*, 2001, **85**, 25–33.
28 Y.-Z. Wang, Q. Liao, X. Zhu, X. Tian and C. Zhang, *Bioresour. Technol.*, 2010, **101**, 4034–4041.
29 J. B. McKinlay, Y. Oda, M. Ruhl, A. L. Posto, U. Sauer and C. S. Harwood, *J. Biol. Chem.*, 2014, **289**, 1960–1970.
30 J. M. Dubbs and F. Robert Tabita, *FEMS Microbiol. Rev.*, 2004, **28**, 353–376.
31 J. B. McKinlay and C. S. Harwood, *Proc. Natl. Acad. Sci.*, 2010, **107**, 11669–11675.
32 K. a. Catchpole and A. Polman, *Opt. Express*, 2008, **16**, 21793–21800.
33 S. Ghasemi, S. Hashemian, A. Alamolhoda, I. Gocheva and S. R. Setayesh, *Mater. Res. Bull.*, 2017, **87**, 40–47.
34 P. Ghosh, G. Han, M. De, C. K. Kim and V. M. Rotello, *Adv. Drug Delivery Rev.*, 2008, **60**, 1307–1315.
35 K.-S. Lee and M. A. El-Sayed, *J. Phys. Chem. B*, 2006, **110**, 19220–19225.
36 C. Loo, A. Lin, L. Hirsch, M.-H. Lee, J. Barton, N. Halas, J. West and R. Drezek, *Technol. Cancer Res. Treat.*, 2004, **3**, 33–40.
37 E. Petryayeva and U. J. Krull, *Anal. Chim. Acta*, 2011, **706**, 8–24.
38 G. Mie, *Ann. Phys.*, 1908, **25**, 377–445.
39 N. Nehru, E. U. Donev, G. M. Huda, L. Yu, Y. Wei and J. T. Hastings, *Opt. Express*, 2012, **20**, 6905–6914.
40 N. Nehru, Y. Linliang, W. Yinan and J. T. Hastings, *IEEE Trans. Nanotechnol.*, 2014, **13**, 55–61.
41 A. Shakiba, S. Shah, A. C. Jamison, I. Rusakova, T.-C. Lee and T. R. Lee, *ACS Omega*, 2016, **1**, 456–463.
42 G. H. Chan, J. Zhao, E. M. Hicks, G. C. Schatz and R. P. Van Duyne, *Nano Lett.*, 2007, **7**, 1947–1952.
43 N. S. Abadeer and C. J. Murphy, *J. Phys. Chem. C*, 2016, **120**, 4691–4716.
44 A. Lishchuk, C. Vasilev, M. P. Johnson, C. N. Hunter, P. Törmä and G. J. Leggett, *Faraday Discuss.*, 2019, **216**, 57–71.
45 A. Lishchuk, G. Kodali, J. A. Mancini, M. Broadbent, B. Darroch, O. A. Mass, A. Nabok, P. L. Dutton, C. N. Hunter, P. Törmä and G. J. Leggett, *Nanoscale*, 2018, **10**, 13064–13073.
46 A. Tsargorodska, M. L. Cartron, C. Vasilev, G. Kodali, O. A. Mass, J. J. Baumberg, P. L. Dutton, C. N. Hunter, P. Törmä and G. J. Leggett, *Nano Lett.*, 2016, **16**, 6850–6856.
47 D. Coles, L. C. Flatten, T. Sydney, E. Hounslow, S. K. Saikin, A. Aspuru-Guzik, V. Vedral, J. K.-H. Tang, R. A. Taylor, J. M. Smith and D. G. Lidzey, *Small*, 2017, **13**, 1701777.
48 B. Wang, K. Xiao, Z. Jiang, J. Wang, J. C. Yu and P. K. Wong, *Energy Environ. Sci.*, 2019, **12**, 2185–2191.
49 A. Pugazhendhi, S. Shobana, D. D. Nguyen, J. R. Banu, P. Sivagurunathan, S. W. Chang, V. K. Ponnusamy and G. Kumar, *Int. J. Hydrogen Energy*, 2019, **44**, 1431–1440.
50 P. T. Sekoai, C. N. M. Ouma, S. P. du Preez, P. Modisha, N. Engelbrecht, D. G. Bessarabov and A. Ghimire, *Fuel*, 2019, **237**, 380–397.
51 H. Zhang, H. Liu, Z. Tian, D. Lu, Y. Yu, S. Cestellos-Blanco, K. K. Sakimoto and P. Yang, *Nat. Nanotechnol.*, 2018, **13**, 900–905.
52 J. Zhao, T. Baba, H. Mori and K. Shimizu, *Metab. Eng.*, 2004, **6**, 164–174.
53 P. B. Johnson and R.-W. Christy, *Phys. Rev. B: Solid State*, 1972, **6**, 4370.
54 E. D. Palik, *Handbook of optical constants of solids*, Academic press, 1998.
55 A. L. Aden and M. Kerker, *J. Appl. Phys.*, 1951, **22**, 1242–1246.